Identification of OAF and PVRL1 as candidate genes for an ocular anomaly characterized by Peters anomaly type 2 and ectopia lentis

David, Dezso

2018-03

David , D , Anand , D , Araujo , C , Gloss , B , Fino , J , Dinger , M , Lindahl , P , Pöyhönen , M , Laivuori , H & Lavinha , J 2018 , ' Identification of OAF and PVRL1 as candidate genes for an ocular anomaly characterized by Peters anomaly type 2 and ectopia lentis ' , Experimental Eye Research , vol. 168 , pp. 161-170 . https://doi.org/10.1016/j.exer.2017.12.012

http://hdl.handle.net/10138/300577
https://doi.org/10.1016/j.exer.2017.12.012

publishedVersion

Experimental Eye Research 168 (2018) 161–170

Contents lists available at ScienceDirect

Experimental Eye Research

journal homepage: www.elsevier.com/locate/yexer

Identification of *OAF* and *PVRL1* as candidate genes for an ocular anomaly characterized by Peters anomaly type 2 and *ectopia lentis*

Dezső David[a,*], Deepti Anand[b], Carlos Araújo[a], Brian Gloss[c,d], Joana Fino[a], Marcel Dinger[c,d], Päivi Lindahl[e], Minna Pöyhönen[f], Laivuori Hannele[g,h], João Lavinha[a]

[a] Department of Human Genetics, National Health Institute Doutor Ricardo Jorge, Lisbon, Portugal
[b] Department of Biological Sciences, University of Delaware, Newark, DE 19716, USA
[c] Genomics and Epigenetics Division, Garvan Institute of Medical Research, Darlinghurst, Australia
[d] St Vincent's Clinical School, Faculty of Medicine, UNSW, Kensington, Australia
[e] Ophthalmology, University of Helsinki and Helsinki University Hospital, Helsinki, Finland
[f] Clinical Genetics, University of Helsinki and Helsinki University Hospital, Helsinki, Finland
[g] Medical and Clinical Genetics, University of Helsinki and Helsinki University Hospital, Helsinki, Finland
[h] Institute for Molecular Medicine Finland, University of Helsinki, Helsinki, Finland

ARTICLE INFO

Keywords:
Balanced chromosome translocation
Keratolenticular dysgenesis
Type 2 peters anomaly
Ectopia lentis
OAF
PVRL1
NECTIN1
Topologically associated domains (TADs)

ABSTRACT

Keratolenticular dysgenesis (KLD) and *ectopia lentis* are congenital eye defects. The aim of this study is the identification of molecular genetic alterations responsible for those ocular anomalies with neurologic impairment in an individual with a *de novo* balanced chromosome translocation t(11;18)(q23.3;q11.2)dn. Disruption of *OAF*, the human orthologue of the *Drosophila oaf*, by the 11q23.3 breakpoint results in reduced expression of this transcriptional regulator. Furthermore, four most likely nonfunctional chimeric transcripts comprising up to *OAF* exon 3, derived from the der(11) allele, have also been identified. This locus has been implicated by publicly available genome-wide association data in corneal disease and corneal topography. The expression of the poliovirus receptor-related 1(*PVRL1*) or nectin cell adhesion molecule 1 (*NECTIN1*), a paralogue of nectin cell adhesion molecule 3 (*PVRL3*) associated with congenital ocular defects, situated 500 kb upstream from 11q23.3 breakpoint, is increased. The 18q11.2 breakpoint is localized between cutaneous T-cell lymphoma-associated antigen 1(*CTAGE1*) and retinoblastoma binding protein 8 (*RBBP8)* genes. Genomic imbalance that could contribute to the observed phenotype was excluded. Analysis of gene expression datasets throughout normal murine ocular lens embryogenesis suggests that *OAF* expression is significantly enriched in the lens from early stages of development through adulthood, whereas *PVRL1* is lens-enriched until E12.5 and then down-regulated. This contrasts with the observation that the proposita's lymphoblastoid cell lines exhibit low *OAF* and high *PVRL1* expression as compared to control, which offers further support that the alterations described above are most likely responsible for the clinical phenotype. Finally, gene interaction topology data for *PVRL1* also agree with our proposal that disruption of *OAF* by the translocation breakpoint and misregulation of *PVRL1* due to a position effect contribute to the observed ocular and neurological phenotype.

1. Introduction

Kerato-irido-lenticular dysgenesis (KILD) is a genetically and phenotypically heterogeneous congenital malformation of the anterior chamber of the eye. This condition, traditionally known as Peters anomaly (PA; OMIM #604229), generally leads to severe visual impairment. PA or KILD is characterized by central corneal opacity or leucoma, adhesion between the central anterior surface of the lens and posterior surface of the cornea with or without iridocorneal adhesions (Nischal, 2015).

Most PA cases are of recessive inheritance and sporadic occurrence, but autosomal dominant inheritance is also reported (David et al., 2003). The prevalence of PA remains unknown and recently the incidence in United States was estimated to be 1.1 to 1.5 per 100,000 live births (Kurilec and Zaidman, 2014). In about two-thirds of cases PA is isolated, and in about 50% it is unilateral (Ozeki et al., 2000).

PA has repeatedly been reported in association with a variety of other ocular malformations (Ozeki et al., 2000). Indeed, genes causing aniridia (OMIM #607108, *PAX6* on 11p13), isolated or syndromic forms of Axenfeld-Rieger syndromes (OMIM #180500 and 602482,

* Corresponding author. Department of Human Genetics, National Health Institute Doutor Ricardo Jorge, Av. Padre Cruz, 1649-016 Lisbon, Portugal.
E-mail address: dezso.david@insa.min-saude.pt (D. David).

https://doi.org/10.1016/j.exer.2017.12.012
Received 20 April 2017; Received in revised form 21 December 2017; Accepted 27 December 2017
Available online 02 January 2018
0014-4835/

PITX2 on 4q25, and *FOXC1* on 6p25.3), and primary congenital glaucoma (PCG, OMIM #231300, *CYP1B1* on 2p22.2), have been observed in association with PA. In addition to these four genes, *MAF*, *FOXE3* and *PITX3* have also been occasionally reported to be involved in PA (Jamieson et al., 2002; Doucette et al., 2011; Summers et al., 2008). Recently, exome sequencing data suggested possible involvement of *TFAP2A*, *HCCS*, *NDP*, *FLNA* and *SLC4A11* in the etiology of PA (Weh et al., 2014). Hence, no specific PA-causing gene has been identified so far. In addition to the well-defined Peters-plus syndrome (OMIM #261540, *B3GALTL* on 13q12.3) other congenital malformations have been reported in association with PA (Ozeki et al., 2000; Mwenda, 2012).

Congenital *ectopia lentis* (EL) is a rare ocular anomaly characterized by dislocation or malposition of the ocular lens (Chandra and Charteris, 2014). This condition occurs predominantly as a manifestation of systemic diseases such as Marfan syndrome (MFS, OMIM #154700, *FBN1* on 15q21). Unilateral EL is often related to trauma or other ocular disorders.

Anterior segment dysgenesis (ASD) disorders including PA have been reported, from time to time, associated with chromosomal abnormalities including reciprocal chromosome translocations (RCT) (David et al., 2003). Indeed, several genes responsible for the genetic etiology of ASD disorders have been identified through breakpoint mapping of chromosomal rearrangements (Mataftsi et al., 2011). This approach continues to be important in the identification of novel genes involved in human developmental disorders (Redin et al., 2017). In fact, by using this approach, in 2003 we identified *TGFB2* as a most likely PA-causing gene (David et al., 2003).

In the present study, we describe a *de novo* balanced RCT [t(11;18)(q23.3;q11.2)dn] in a subject with KLD (or type 2 PA) in the right eye, *ectopia lentis* in the left eye, and neurological impairment. Identification of the breakpoints at nucleotide resolution, comprehensive molecular analysis of the flanking genomic regions, and potential candidate gene search in the light of chromatin topologically associated domains (TADs), reinforced by gene expression data during normal murine ocular lens embryogenesis lead us to conclude that disruption of *OAF* by the translocation breakpoint and developmental misregulation of *PVRL1*, are the main molecular alterations most likely responsible for the phenotype observed in this subject.

2. Materials and methods

2.1. Samples, lymphoblastoid cell lines (LCLs), chromosome painting and fluorescence in-situ hybridization (FISH) mapping

Blood samples from the proposita and her relatives were collected after informed consent. The study was carried out according to the Principles of the Declaration of Helsinki of the World Medical Association. Establishment of LCLs from peripheral blood lymphocytes, whole chromosome painting (WCP) and FISH mapping, were performed as previously described (David et al., 2003, 2013).

2.2. DNA extraction, flow sorting of derivative (der) chromosomes, genomic amplification, array painting and genomic array analysis

Genomic DNA extraction from peripheral blood lymphocytes and LCLs, flow sorting and amplification of DNAs from der(11) and der(18) chromosomes were performed as described (David et al., 2013).

Total genomic DNA from the proposita and the genomic amplicon of der(11) were analyzed using high-resolution CytoScan HD genomic array from Affymetrix (Santa Clara, CA, USA), performed according to the manufacturer's instructions. Array data were analyzed using the chromosome analysis suite (ChAS) software and NetAffy Genomic Annotation file version 33.1 hg^{19}, from Affymetrix. Potential alterations or CNVs were queried in the Database of Genomic Variants (DGV; http://dgv.tcag.ca/dgv/app/home).

2.3. Amplification of the junction fragments and mutation screening of CYP1B1

Amplification conditions for the der(11) and der(18) junction fragments, with primer pairs OAF-5F/AC110583-7R and AC110583-8F/AP000679-2R, respectively are summarized in Supplementary Table S1. The resulting junction fragments were sequenced by the Sanger method (David et al., 2013). For details regarding mutation screening of *CYP1B1* see Supplementary material.

2.4. RNA extractions and expression studies

Extraction of RNA from LCLs and peripheral blood of the proposita, family members and controls as well as quality assessment and quantification of RNAs were performed as described earlier (David et al., 2013).

Genome-wide assessment of gene expression levels in LCL of the proposita and controls were performed using the Human Gene 1.0 ST expression array from Affymetrix according to the manufacturer's instructions. Data from eight unrelated LCL samples were used as controls and the analysis was performed using the Chipster v3.6 open source platform (http://chipster.csc.fi/). For additional details, see Supplementary material.

Expression levels of several genes mapping to the breakpoint regions were analyzed by TaqMan gene expression assays. The information regarding these genes, assays, amplicons, amplification conditions and relative quantification of target genes are available in Supplementary material and Table S2.

Transcripts from reference genomic regions, equivalent to the breakpoint-spanning and flanking TADs from each breakpoint, were enriched using capture probe libraries. The probes were designed by Roche-Nimblegen using Custom SeqCap EZ design for hg19 regions covering the reference TADs (Supplementary Table S3). Regions covering TAD boundaries, VISTA enhancers, candidate genes and breakpoints were more densely tiled. Probes were allowed up to 20 close matches in the genome. Probes to capture 50 External RNA Control Consortium (ERCC) controls were also added. Approximately 8.5% of the selected regions were untargetable due to repeats. Of the remaining, a median coverage of 95% was achieved. Capture was performed on cDNA libraries prepared from 100 ng total RNA as previously described (see Supplementary material) (Mercer et al., 2014). The average clone size in the enriched pooled library was 345 bp. Sequencing was performed using the Illumina HiSeq2500 platform and version 4 chemistry for cluster generation, and sequenced with 150 bp paired-end sequencing. RNA CaptureSeq data analysis can be found in Supplementary material.

2.5. Meta-analysis of mouse expression array datasets

For expression analysis of mouse orthologues of the identified potential human candidate genes during normal murine ocular lens embryogenesis, publicly available genome-wide mouse expression array datasets were used.

Expression and enrichment in lens tissue of mouse orthologues was obtained by comparison of fluorescent expression intensities at embryonic day (E) E10.5, E11.2, E12.5, E16.5 and E17.5, and postnatal day (P) P0 and P56 stages to reference whole body (WB) controls, as previously described (Agrawal et al., 2015).

Similarly, expression and enrichment in the isolated lens epithelium at P28 for the *Oaf* and *Pvrl1* genes was obtained by analyzing the specific probe signal intensity. Comparative analyses of these two genes with the whole body embryonic tissue (WB) reference dataset, expressed as fold-change differences, provided an estimate of their “enriched” expression in the P28 lens epithelium. For additional information regarding the source mouse expression array datasets and analyses, see Supplementary material.

2.6. Topologically associated domain (TAD) data

Hi-C chromatin interaction maps from the analyzed TADs or gene regions were generated for the human embryonic IMR90 fibroblast cell line (ATCC CCL-186) and human LCL GM12878 with *Mbo*I digestion from the publicly available GEO GSE63525 dataset (https://www.ncbi.nlm.nih.gov/geo/query/acc.cgi?acc=GSE63525) (Rao et al., 2014).

For detailed bioinformatics analysis of Hi-C sequencing libraries, heat maps of Hi-C chromatin interactions and Circos plot of gene interaction profiles please see Supplementary material.

3. Results

3.1. Clinical and ophthalmological features

The proposita is the third child of non-consanguineous parents. Her father has congenital nystagmus, but otherwise her parents as well as her siblings are healthy. At birth, she was small and hypotonic and required assisted ventilation. Her parents noticed a grey dot in the right eye. Motor development was slower compared to her siblings. She learned to walk properly at the age of three years. No dysmorphic features were noted.

Ophthalmologic examination performed at four years and ten months of age revealed microphthalmic eyes with secondary developmental KLD or type 2 PA in her right eye (OD), the lens with anterior cataract adherent to the centrally opacified cornea, and inferonasal subluxation of the lens in her left eye (OS) (Fig. 1). In the right eye there were some fine iris strands and vessels attached to lens epithelium but no pupillary membrane or persistent fetal vasculature causing mechanical lens-cornea adhesion. Medical history shows that there was no additional report of ASD in her family.

At six years of age, the lens and the cornea were clear in the OS with inferonasal subluxation of the lens. The posterior segment was normal. Visual acuity was low because of bad optics due to lens subluxation. The OS was submitted to lens extraction with repositioning of the lens capsule with transsclerally fixated capsular tension ring and intraocular lens (IOL) implantation. Vision improved from 0.08 to 0.4.

At seven years of age, the axial length of the OD was 18.44 mm (normal average 22 mm ± 0.61). Visual acuity before cataract operation was 0.1 (20/200 or 6/60). The cornea was clear at the periphery but cloudy in the optic axis due to adhesions between the lens and corneal endothelium. The lens had an anterior, pyramid-shaped opacification to which some vessels grew from the inferonasal atrophic iris. The pupil did not react properly to light. The posterior segment of the eye (retina, optic nerve) was normal. At this age, the OD was submitted to excision of lenticulocorneal adhesion, extracapsular cataract extraction (ECCE) and IOL implantation. Visual acuity improved marginally (0.2) due to deep amblyopia.

Neurological evaluation at four and a half years revealed motor clumsiness or coordination problems, repeatedly abnormal electroencephalogram (spikes in two independent foci in the occipital region) and slightly exaggerated signals from the nucleus caudate on magnetic resonance imaging examination. At the age of four she spoke relatively fluently, but stuttered and she received speech and physical therapy.

3.2. Cytogenetic studies

Analysis of GTL-banded metaphase chromosomes revealed in the proposita an apparently balanced reciprocal chromosomal translocation between the long arms of chromosomes 11 and 18 46,XX,t(11;18)(q25;q11.2)dn (Supplementary Figs. S1a and b). The *de novo* (dn) nature of the translocation was demonstrated by the fact that the karyotypes of the proposita's parents were normal.

3.3. Mapping of the breakpoints at nucleotide resolution and identification of candidate genes

First, breakpoint-spanning BAC clones were identified (Supplementary Figs. S1d and S2b). The 11q25 breakpoint was further delimited by FISH mapping of long-range PCR fragments. A 7.75 kb fragment (g.OAF4/AP11503) encompassing *OAF* exons 2–4 was identified as the shortest breakpoint-spanning FISH probe (Supplementary Figs. S2c and d).

Subsequently, der-chromosomes were separated from their normal counterparts by dual-laser flow sorting and breakpoints were more precisely localized by array painting with the der(11) amplicon (Supplementary Figs. S1e–g).

Primers flanking the breakpoints were designed, and junction fragments amplified, and Sanger sequenced (Supplementary Table S1 and Fig. S3). According to the next-gen cytogenetics nomenclature, the breakpoints can be defined as: seq[hg38] t(11;18)(11pter- > 11q23.3(120,227,15{9}):18q11.2(22,640,75{1})- > 18qter; (18pter- > 18q11.2(22,640,751):11q23.3(120,227,159)- > 11qter)dn (Ordulu et al., 2014). The translocation, according to the International System for Human Cytogenetic Nomenclature (ISCN) 2016, is defined as seq[GRCh38] t(11;18)(11pter→11q23.3:18q11.2 → 18qter;18pter→ 18q11.2:11q23.3 → 11qter)dn.

The 11q23.3 breakpoint was identified at position g.120,227,159_120,227,160 [hg38] within IVS3 of *OAF*, the human orthologue of the *Drosophila "out at first"* (*oaf*) (Supplementary Figs. S2c and S3). Based on FANTOM CAT browser data on genome wide association studies (GWASs; http://fantom.gsc.riken.jp/cat/v1/#/genes/ENSG00000184232.4) the *OAF* locus has been associated with corneal disease, and corneal topography (rs2444239, at position120,185,707; p = 4.500E-07 and rs494965, at position 120,182,942; p = 4.00E-7).

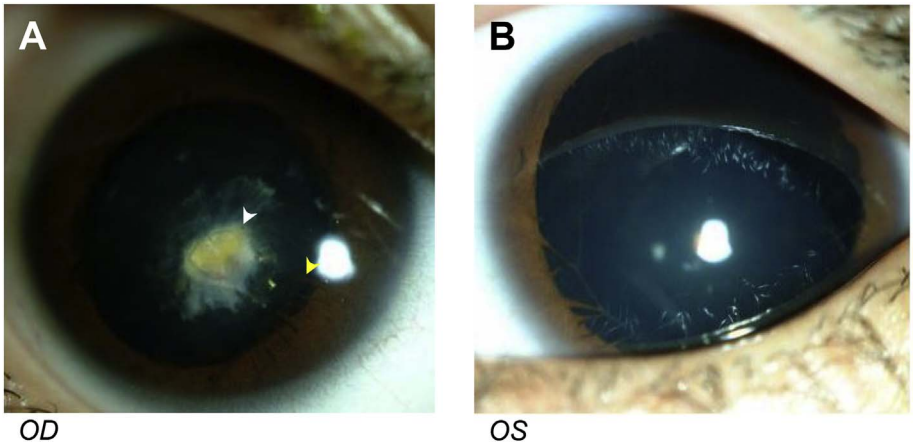

Fig. 1. Ocular phenotype of the proposita.
A) *Oculus dexter* (OD) before ocular surgery; microphthalmic eye with congenital keratolenticular dysgenesis or type 2 Peters anomaly (type 2 PA). The lens presents an anterior, pyramid-shaped opacification (white arrowhead) to which some fine iris strands (yellow arrowhead) and vessels grew from the inferonasal atrophic iris. The cornea is clear at the periphery but cloudy in the optic axis due to adhesions between the lens and corneal endothelium.
B) *Oculus sinister* (OS) before ocular surgery; microphthalmic eye with inferonasal subluxation of the lens. Otherwise the lens and the cornea are clear.

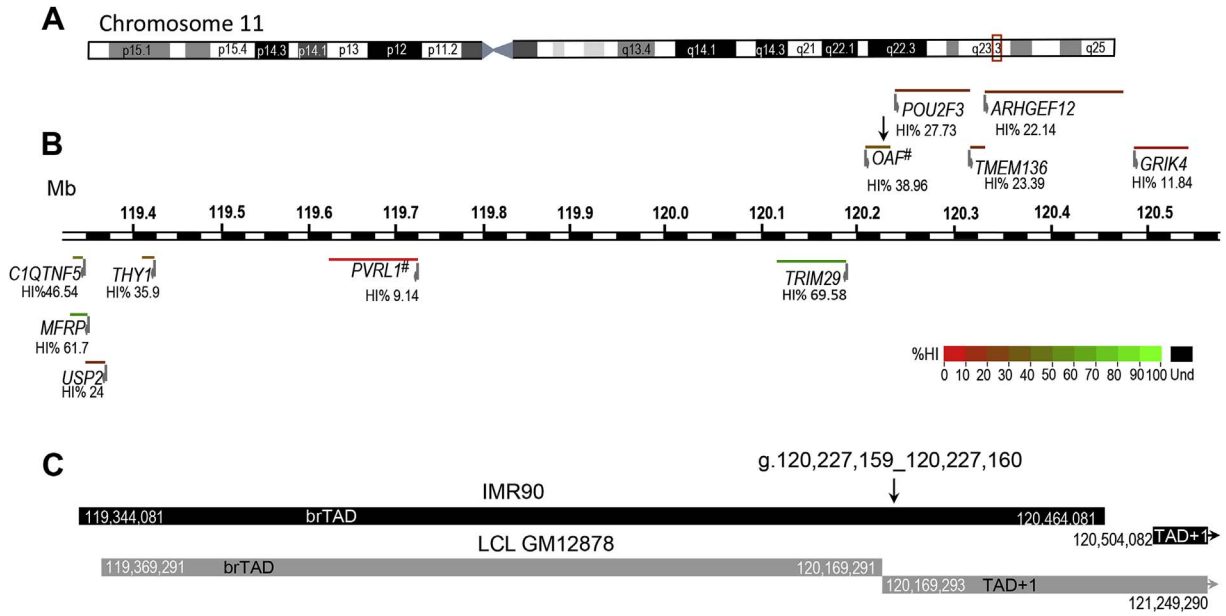

Fig. 2. Ideogram of chromosome 11, physical gene map and TADs within the breakpoint region. **A)** Schematic ideogram of chromosome 11; the breakpoint region is highlighted by a red box. **B)** Detailed gene map across the 11q23.3 breakpoint region. Horizontal lines with arrowheads indicate the position of genes in sense (above the map) and antisense (below the map) orientation. Genes are color-coded according to their haploinsufficiency index (HI) available at https://decipher.sanger.ac.uk/and the HI score is indicated below. Most important candidate genes are marked with a hash mark (#). Arrows indicate the breakpoint position within *OAF*. **C)** Topologically associated domains across the breakpoint. The TADs in human IMR90 fibroblasts (IMR90) and LCLs GM12878 are shown below [hg38].

Proximally, the breakpoint is flanked by a member of the tripartite motif (TRIM) proteins family, *TRIM29*. About 10 kb distal from this location lies the gene encoding POU domain, class 2 transcription factor 3 (*POU2F3*), also known as octamer-binding transcription factor 11 (*OCT11*). About 100 kb further distal, maps the Rho guanine nucleotide exchange factor 12 (*ARHGEF12*). Additional functionally important genes are localized within the reference IMR90 breakpoint-spanning TAD (brTAD). Among these genes is poliovirus receptor-related 1 (*PVRL1*) also known as *NECTIN1*, a member of the Ca^{2+}-independent immunoglobulin-like cell adhesion molecules, localized about 500 kb proximal to the breakpoint (see Fig. 2B). A paralogue of this cell adhesion protein, *PVRL*3, was recently shown to have an important role in mammalian lens and ciliary body development. Misregulation of *PVRL3* expression by t(1;3)(q31.3;q13.13) translocation also leads to congenital ocular defects in human and its targeted deletion in mice causes severe eye defects (Lachke et al., 2012). Mutations affecting *PVRL1* have been reported to cause autosomal recessive cleft lip/palate-ectodermal dysplasia syndrome (CLPED1; OMIM #225060) and a form of orofacial cleft (OFC7) (OMIM #225060) (Suzuki et al., 2000). Interaction plots depict extensive interactions between *OAF* or the breakpoint region and *PVRL1* (Fig. 3).

These adhesion proteins (PVRL1 and 3) are direct interacting partners, mediating apex-apex adhesion between the anterior lens epithelium and fiber cells, as well as between pigmented and non-pigmented cell layers of the ciliary body epithelium (Lachke et al., 2012). Additionally, are also expressed in the brain at synaptic junctions and *puncta adherentia* junctions (Takai et al., 2003). Both are down regulated during TGFB induced epithelial-mesenchymal transition, known to play an important role in the pathogenesis of ASD (Li et al., 2016; http://fantom.gsc.riken.jp/cat/v1/#/). *PVRL1* expression is reduced by a maximum fold change (MFC) of −1.87 with a false discovery rate (FDR) of 0.0438, whereas *PVRL3* expression has a MFC of −1.94 and FDR of 0.0248 (http://fantom.gsc.riken.jp/cat/v1/#/).

Two additional genes involved in ocular pathologies are located at the boundary between TAD-1 and brTAD of the 11q23.3 breakpoint (Fig. 4). The first is the membrane frizzled-related protein gene (*MFRP*) whose mutations cause microphthalmia isolated 5 (MCOP5; OMIM #611040) and nanophthalmos 2 (NNO2; OMIM #609549). The second gene is the complement-C1q tumor necrosis factor-related protein 5 (*C1QTNF5)* associated to late-onset autosomal dominant retinal degeneration (LORD; OMIM #605670).

The 18q11.2 breakpoint was localized at position g.22,630,751_22.640,752 [hg38] and a 13 bp duplication (TACAGAG ATGTAC) of the chromosome 11 sequence was identified at the breakpoint junction (Supplementary Fig. S3). This breakpoint is localized within the intergenic region of genes involved in tumorigenesis, namely cutaneous T-cell lymphoma-associated antigen 1(*CTAGE1*) and retinoblastoma binding protein 8 (*RBBP8*) also known as CtBP-interacting protein (CtIP) (Supplementary Figs. S4 and S5). The first is localized within the brTAD, about 270 kb proximal to the breakpoint and is associated with cutaneous T-cell lymphoma. Within the same TAD is localized a member of the small family of zinc finger factors, the GATA6 binding protein 6 (*GATA6*). This gene is associated with several autosomal dominant congenital heart defects (OMIM #614474, #614475, #187500, #217095 and #600001). However, no heart defect has been reported in the proposita. Distally, the breakpoint-flanking *RBBP8* gene is situated in the adjacent TAD (TAD + 1) at 235 kb, and has been associated with autosomal recessive Seckel and Jawad (dysmorphic) syndromes (SCKL2, OMIM #606744; JWDS, OMIM #251255) (Qvist et al., 2011). On the contrary of *RBBP8* neither of the breakpoint flanking genes (*CTAGE1 and GATA6*) display significant interactions across the breakpoint (Supplementary Fig. S5 and S6a-c). Presently, none of these genes from 18q11.2 are considered as a candidate for this ocular anomaly (Supplementary Fig. S5).

Computational prediction of Phenomatch score, MaxPhenoScore and Pheno_percentile, that define the similarity between the proposita's phenotype and those clinical traits associated with genes from the breakpoint regions, and position effect prediction scores were calculated according to a recently reported method (Zepeda-Mendoza et al., 2017). A significant Pheno_percentile of 0.84 (significant if > 0.75) and the highest prediction score of 3 (maximum score is 5) was obtained for *PVRL1*. Presently, OAF is not linked to any phenotype; therefore, no phenomatch score could be obtained.

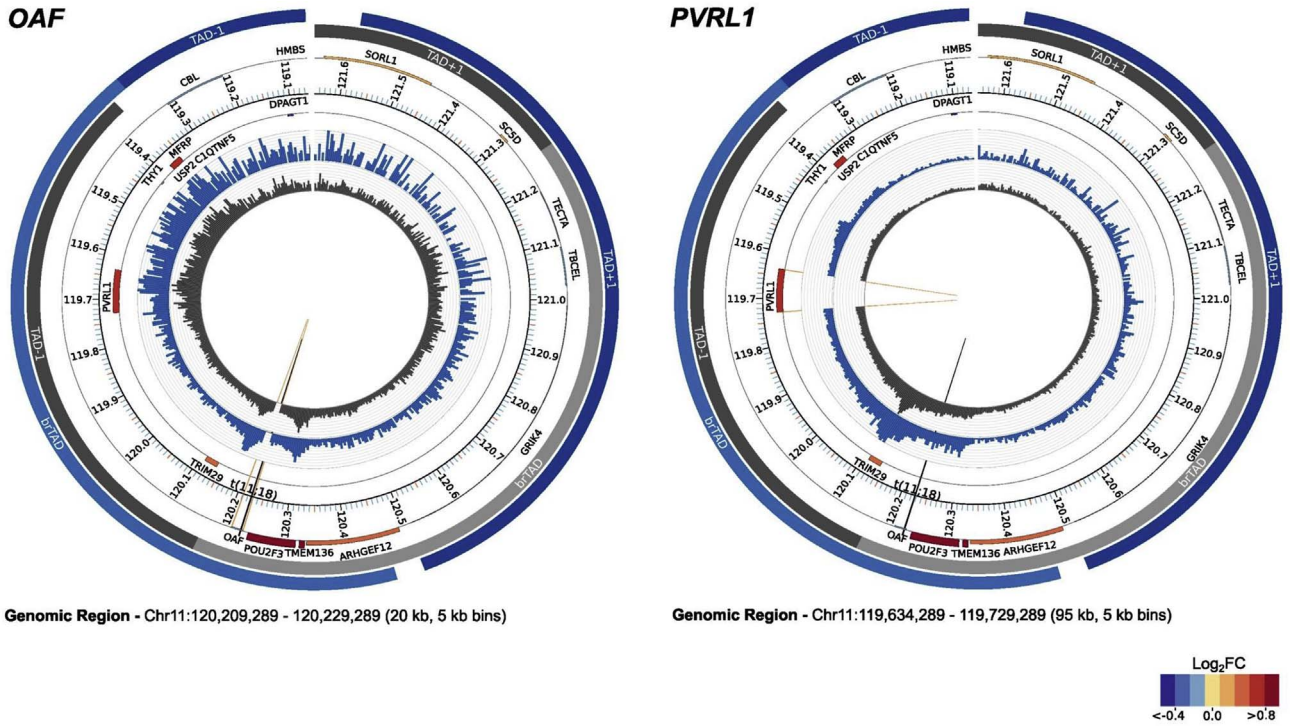

Fig. 3. Circos plot of interaction profiles of main candidate genes *OAF* and *PVRL1* from the 11q23.3 breakpoint in IMR90 fibroblasts and LCLs GM12878. The blue and dark grey outer tracks depict TADs in IMR90 and LCLs, respectively. The analyzed gene regions are highlighted by tawny lines whereas the position of translocation breakpoint is indicated by a black line. Color-coded histograms show the gene expression levels in LCLs, and are depicted in sense (above the map) and antisense (below the map) orientation. In the inner circles, interaction frequencies between each gene and the reference genomic region are depicted in the blue and black histograms, for the IMR90 and LCL, respectively.

3.4. Mutation screening of *CYP1B1* and unbalanced genomic alterations

The proposita was screened for mutations within *CYP1B1* and for genomic imbalances. Neither mutations within *CYP1B1*, nor genomic imbalances affecting *CYP1B1* or the breakpoint regions, were observed. The imbalances identified elsewhere in the genome are most likely CNVs (Supplementary Table S4).

3.5. Expression studies

First, Human Gene 1.0 ST expression array profiling of LCLs of the proposita revealed two genes, cytochrome P450 family 1 subfamily B polypeptide 1 (*CYP1B1* on 2p22.2) and EGF-like repeats and discoidin domains 3 (*EDIL3* on 5q14), with highly significant altered expression as compared to controls. Consequently, a 16.5-fold decrease and 126-fold increase, respectively, was confirmed by TaqMan expression assay (Table 1 and Fig. S7). The association of CYP1B1 dysfunction with ocular pathologies, including PA, is well known (Vincent et al., 2006). Therefore, the *CYP1B1* expression level was also analyzed in the peripheral blood of the proposita; the expression level was not significantly different from the controls (*CYP1B1* fold change $2^{-\Delta\Delta Cq} = 3.048 \pm 0.164$ vs. 4.256 ± 0.517). Furthermore, the reduction observed in the proposita's LCLs was compared with *CYP1B1* expression levels from LCLs with a homozygous as well as a heterozygous 13-nt deletion in *CYP1B1* exon 3 (data not shown). This suggests that the observed reduction in expression observed exclusively in the proposita's LCLs is insufficient to be considered as pathogenic.

The expression level of genes mapping to both breakpoint regions was also analyzed. Compared to the controls, those from the 11q23.3 brTAD are increased whereas those from the 18q11.2 brTAD are not notably different (Table 1; Fig. 4 and S5). Subsequently, most of these genes were also analyzed by TaqMan expression assay (Supplementary Fig. S8). With exception of the *OAF*, disrupted by the breakpoint, expression results were concordant. As expected, the allele-specific *OAF* expression assay shows a reduction of the expression level from the allele disrupted at exons 3-4 junction.

Subsequently, we also carried out RNA CaptureSeq of samples from peripheral blood and LCLs of the proposita and controls, across the reference TAD regions. RNA CaptureSeq results are presented as a heat map of log2 CPMs (counts per million; Supplementary Fig. S9). Expression profiles between blood and LCL samples were significantly different.

In addition to the wild-type *OAF* transcripts, four different chimeric transcript isoforms have also been identified (Fig. 5). As all chimeric transcripts utilize the consensus splice donor/acceptor dinucleotide sequences, they cannot be considered as artifacts. Theoretically, the chimeric OAF variant consists of a 66 amino acids polypeptide encoded by *OAF* exons 2 and 3 followed by an additional pentapeptide encoded by the chromosome 18 derived sequence. This variant is most likely degraded.

Hypothetical candidate genes from both breakpoint regions were then analyzed for their expression during normal murine ocular lens development at various embryonic stages from E10.5 to E17.5, at postnatal day P0 and P56, as well as in isolated mouse lens epithelium at P28. The mouse orthologue of the *OAF* candidate gene, disrupted in the proposita by the 11q23.3 breakpoint, exhibits high expression as early as E10.5, and progressively elevated expression throughout the analyzed stages. Furthermore, its expression is significantly enriched in the lens and in isolated mouse lens epithelium at P28 (Fig. 6). Previously, significant lens-enrichment has led to the identification of several new genes linked to ocular developmental defects (Agrawal et al., 2015; Lachke et al., 2012). On the contrary, *Pvrl1* is expressed from E10.5 to E12.5 and is down-regulated at later stages. It is only enriched in the E11.5 and E12.5 lens as compared to the WB reference dataset. Furthermore, *Oaf* is expressed and enriched at several-fold higher levels in mouse lens epithelium as compared to *Pvrl1*.

Three of the analyzed genes from 11q23.3, namely *ARHGEF12*, *USP2* and *TMEM136*, exhibit significantly enriched expression patterns

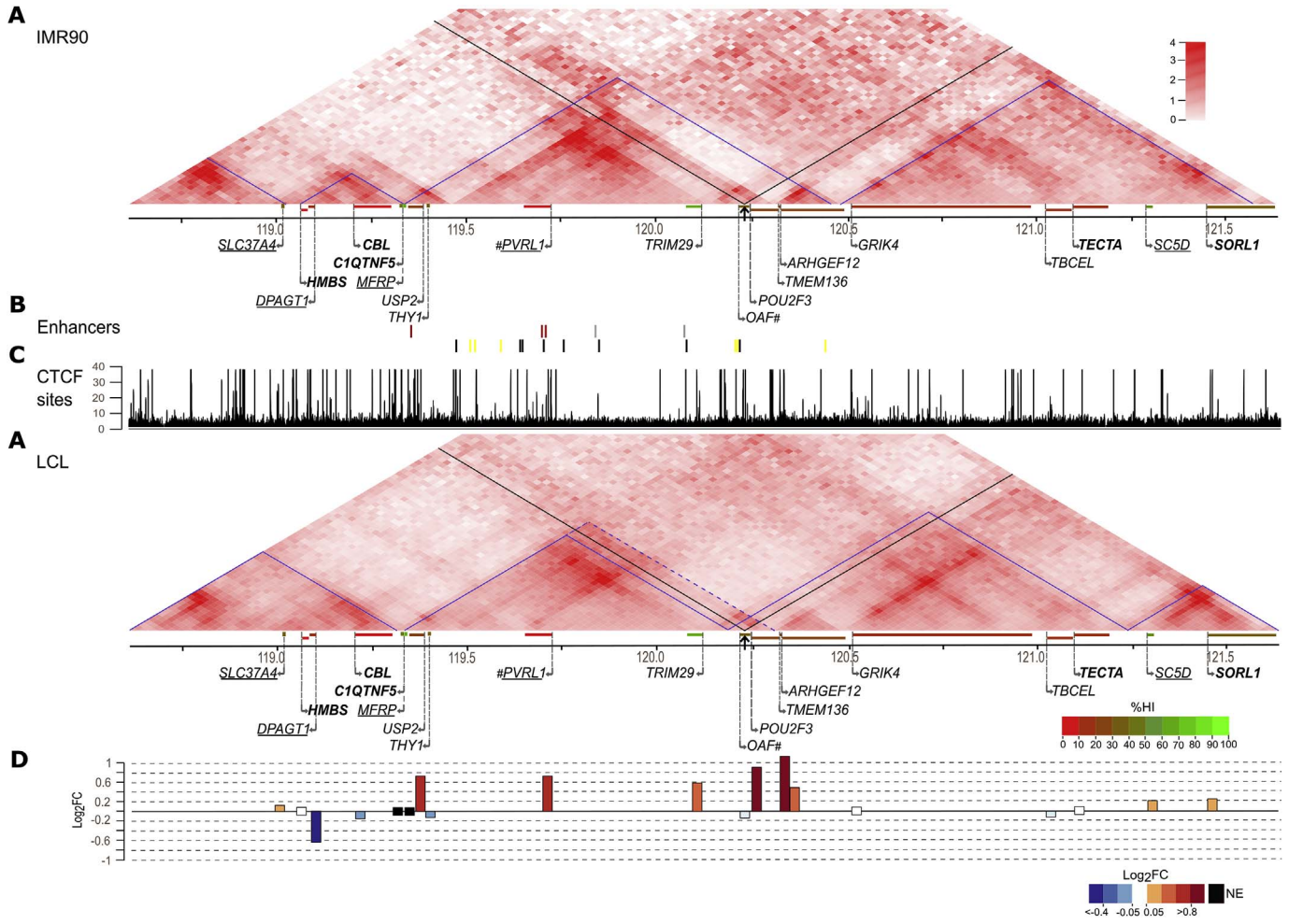

Fig. 4. Heat maps of the 11q23.3 breakpoint region.

A) Hi-C chromatin interaction heat maps for IMR90 fibroblasts and LCL GM12878, respectively. Heat maps were generated from publicly available GEO GSE63525 datasets (https://www.ncbi.nlm.nih.gov/geo/query/acc.cgi?acc=GSE63525). TADs and boundaries are indicated by the overlaid blue lines and are in agreement with published data. According to the interaction profile of this breakpoint region in LCL, the revised breakpoint-spanning topologically associated domain (brTAD) boundary is depicted by the blue dashed line. The black overlaid lines and arrows indicate the 11q23.3 breakpoint. Gene map across the analyzed genomic region is shown below. Forward and reverse arrowheads indicate the position of genes in sense or antisense orientation. Genes are color-coded according to their haploinsufficiency index (HI) available at https://decipher.sanger.ac.uk/. All protein coding genes within the bpTAD are indicated whereas in adjacent TADs only genes proposed to be associated with human disorders are indicated. Genes presently associated with autosomal dominant disorders are in bold, whereas those associated with autosomal recessive disorders are underlined. Candidate genes are indicated by a hash mark(#).

B) Transcribed human enhancers (http://enhancer.binf.ku.dk/enhancers.php) from the reference genomic regions are shown color coded according to their tissue and cell specific expression: in dark red (▮) eye tissue with or without retinal pigment epithelial cells; in grey (▮) nervous system; in yellow (▮) immune system; in black (▮) ubiquitous expression. Three intergenic eye-specific expressed human enhancers have been identified. One is localized within the *USP2* and two within the *PVRL1*. Additional brain specific enhancers have also been identified proximal to the 11q23.3 breakpoint.

C) Track depicting CCCTC-binding factor (CTCF) sites from the analyzed region according to Chip-seq track in the IMR90 fibroblasts (IMR90 CTCF IgG-rab ChIP-seq Signal from ENCODE/SYDH; ENCODE Project Consortium).

D) Color-coded bar plot with the average fold change (Log_2FC) of indicated genes. White bars depict genes with FC between −0.05 and 0.05. Black bars indicate genes without expression in LCLs.

throughout the analyzed mouse lens stages (Supplementary Fig. S10). From 18q11.2, only *RBBP8* exhibits significant expression without enrichment in mouse lens between E10.5 through E17.5.

3.6. Breakpoint regions in the context of TADs

The identification of TADs, whose disruption may contribute to the pathogenic effect of balanced chromosome rearrangements, prompted us to analyze our data in the context of these genomic interaction domains (Lupiáñez et al., 2015). Total, disrupted and maintained intrachromosomal interactions of reference TADs from both breakpoint regions are presented in Supplementary Table S5.

The 11q23.3 breakpoint region displays a considerable level of heterogeneity between TAD boundaries in the two analyzed cell lines. This is associated with the absence of a clear correlation between boundary regions and CCCTC-binding factor (CTCF) sites (Fig. 4). Although *OAF* and *PVRL1* are located within the same TAD only in the IMR90 fibroblasts, the interaction profile of *PVRL1* observed in LCLs suggests that the brTAD boundary may well be further distal from the established TAD boundary (Fig. 4). The *CBL* and *TECTA* genes, localized in adjacent TADs and associated to autosomal dominant conditions, are not involved in significant interactions across the breakpoint (Supplementary Fig. S11f and g).

In IMR90 fibroblasts, the 18q11.2 brTAD is the first centromeric TAD on the long arm. In this region, TAD boundaries are observed to be relatively constant between cell lines and associated with the presence of CTCF-binding sites (Supplementary Fig. S5). This implies that the breakpoint does not substantially affect homeotic chromatin architecture at the 18q11.2 locus.

Transcribed human enhancers (FANTOM, http://enhancer.binf.ku.

Table 1
Summary of gene expression data obtained by different methods.

Gene	[a]Predominant expression	[b]Mouse lens	Assay	Proband		Desc. Statistics	
				[c]Log2	[d]Value	Average	SD
11q23.3 region							
USP2	Skeletal muscle, testis	SignExp& Enrich	HuGene-1.0	0.73	6.02*	5.34	0.21
			CapRNASeq	4.15	5.33*	1.18	2.21
PVRL1	Esophagus mucosa, Skin	SignExp& Enrich	HuGene-1.0	0.98	8.19*	7.28	0.29
			CapRNASeq	1.87	12.04*	10.17	0.63
			RT-qPCR	0.48	1.04*	0.87	0.53
TRIM29	Esophagus mucosa, Skin	Not Sign Exp&Enrich	HuGene-1.0	0.59	6.84*	6.19	0.20
			CapRNASeq	4.53	7.09*	2.56	1.93
OAF	Liver	SignExp& Enrich	HuGene-1.0	0.10	6.99	6.79	0.21
			CapRNASeq	0.77	7.34	6.57	0.90
			RT-qPCR	−0.37	0.12	0.21	0.15
POU2F3	Skin	Not analyzed	HuGene-1.0	0.28	7.29	7.0	0.40
			CapRNASeq	1.62	7.32	5.71	1.43
			RT-qPCR	1.55	0.51	0.29	0.34
TMEM136	Brain	SignExp& Enrich	HuGene-1.0	0.44	6.86	6.5	0.37
			CapRNASeq	0.04	8.12	8.08	0.72
			RT-qPCR	1.84	0.36*	0.18	0.11
ARHGEF12	Brain	SignExp& Enrich	HuGene-1.0	0.30	9.55	9.27	0.26
			CapRNASeq	0.00	12.06	12.06	0.35
			RT-qPCR	0.69	0.59*	0.37	0.15
18q11.2 region							
GATA6	Ovary	Not Sign Exp&Enrich	HuGene-1.0	0.01	6.67	6.66	0.13
			CapRNASeq	−0.59	1.26	1.85	1.01
CTAGE1	Testis	Not analyzed	HuGene-1.0	−0.11	3.73	3.70	0.10
			CapRNASeq	−3.39	−9.97	−6.57	4.22
RBBP8	Kidney, Testis	SignExp	HuGene-1.0	−0.05	9.38	9.43	0.27
			CapRNASeq	−0.18	11.03	11.21	0.35
CYP1B1	Tibial nerve	Not analyzed	HuGene-1.0	−3.45	6.05*	9.51	0.90
			RT-qPCR	−3.59	0.08	1.31	1.2
EDIL3	Brain, arteries	Not analyzed	HuGene-1.0	5.91	9.83	3.88	0.35
			RT-qPCR	14.51	0.147**	0.0012	0.004

[a]According to Genotype-Tissue Expression (GTEx) dataset http://www.gtexportal.org/home/and [b]mouse lens expression datasets (see the Results section and Fig. 6 and Supp. Fig. S10). Array dada are expressed in log2FC[c] and normalized expression level[d] (NEL); RNA CaptureSeq data is reported as log2FC[c] (proband vs. Controls) and log2 CPM + 0.001[d]; and TaqMan RT-qPCR assay in 2^-ΔΔCq[c] and 2^-ΔCt[d]. One asterisk indicates difference greater than 1.5 SD whereas two asterisks indicate statistical significance.
Significantly expressed and enriched: SignExp&Enrich; Significantly expressed: SignExp; Not significantly expressed or enriched: Not SignExp&Enrich.

dk/enhancers.php) from the reference genomic regions are summarized in Fig. 4, and Supplementary Figs. S5 and S12. About 54 kb distal from the 18q11.2 breakpoint a significantly expressed enhancer in retinal, lens and iris derived cells was identified. Additional epithelial cell specific enhancers are also present in this genomic region (Supplementary Fig. S12).

4. Discussion

We report the balanced chromosome translocation t(11;18)(q25;q11.2)dn in association with an ocular anomaly characterized by developmental KLD or type 2 PA (*OD*), *ectopia lentis* (*OS*) and mild CNS abnormalities. As recently reported by Redin et al. a causal relationship between a congenital anomaly and an associated balanced chromosomal rearrangement is expected to occur in up to 40% of the affected subjects (Redin et al., 2017).

Exclusion of the pathogenic significance of reduced *CYP1B1* expression observed exclusively in the proposita's LCLs and of genomic imbalances, reinforced the notion of the proposita's phenotype being the result of functional impairment of the genes (directly or indirectly) affected by the translocation. Therefore, comprehensive structural and functional analyses of the breakpoint regions and adjacent genes were undertaken.

The only gene disrupted by the breakpoints is *OAF*, the human orthologue of the *Drosophila oaf*. Homozygosity for transposon-induced *oaf* mutations led to lethality at late embryogenesis or at first instar larva stage. Mutant embryos show nervous system defects suggestive of its involvement in proper neuronal development (Bergstrom et al., 1995). Expression studies confirmed the presence of *oaf* transcripts in central nervous system (CNS), at stage-15 and 16 (Mukai et al., 2006).

The human OAF is a mature protein of 246 amino acids that shares 38.7% identity and 55.8% similarity with the *Drosophila* oaf. Reported FANTOM CAT (http://fantom.gsc.riken.jp/cat/v1/#/) data on *OAF* highlight its possible involvement in corneal development. Abnormal placement of pupils, failure of eyelids to open and abnormal retinal pigmentation have been reported in *Oaf* knockout mice (http://www.mousephenotype.org/data/genes/MGI:94852#section-associations). Furthermore, high OAF protein level was reported in vitreous humor of the eye (http://www.genecards.org/cgi-bin/carddisp.pl?gene=OAF). However, a 69.5-kb deletion encompassing the entire *OAF* (variant nsv518464, http://dgv.tcag.ca/dgv/app/variant?id=nsv518464&ref=NCBI36/hg18) was identified in an apparently disease-free subject. We propose *OAF* as a strong candidate contributing to the observed phenotype.

Knockout of either cell-adhesion proteins PVRL1 or PVRL3 in the mouse results in virtually identical microphthalmic ocular phenotypes (Inagaki et al., 2005). Furthermore, disruption of *PVRL3* causes bilateral congenital cataracts and mild developmental delay (Lachke et al., 2012). Computational prediction of position effect and of phenotype similarity (phenomatch) also corroborate the involvement of *PVRL1* in this phenotype. Additional cell adhesion and polarity proteins, such as cadherins, protein kinase C lota (*PRKCI*) and signal-induced proliferation associated 1 like 3 (*SIPA1L3*), have been reported to cause abnormal lens development including bilateral congenital

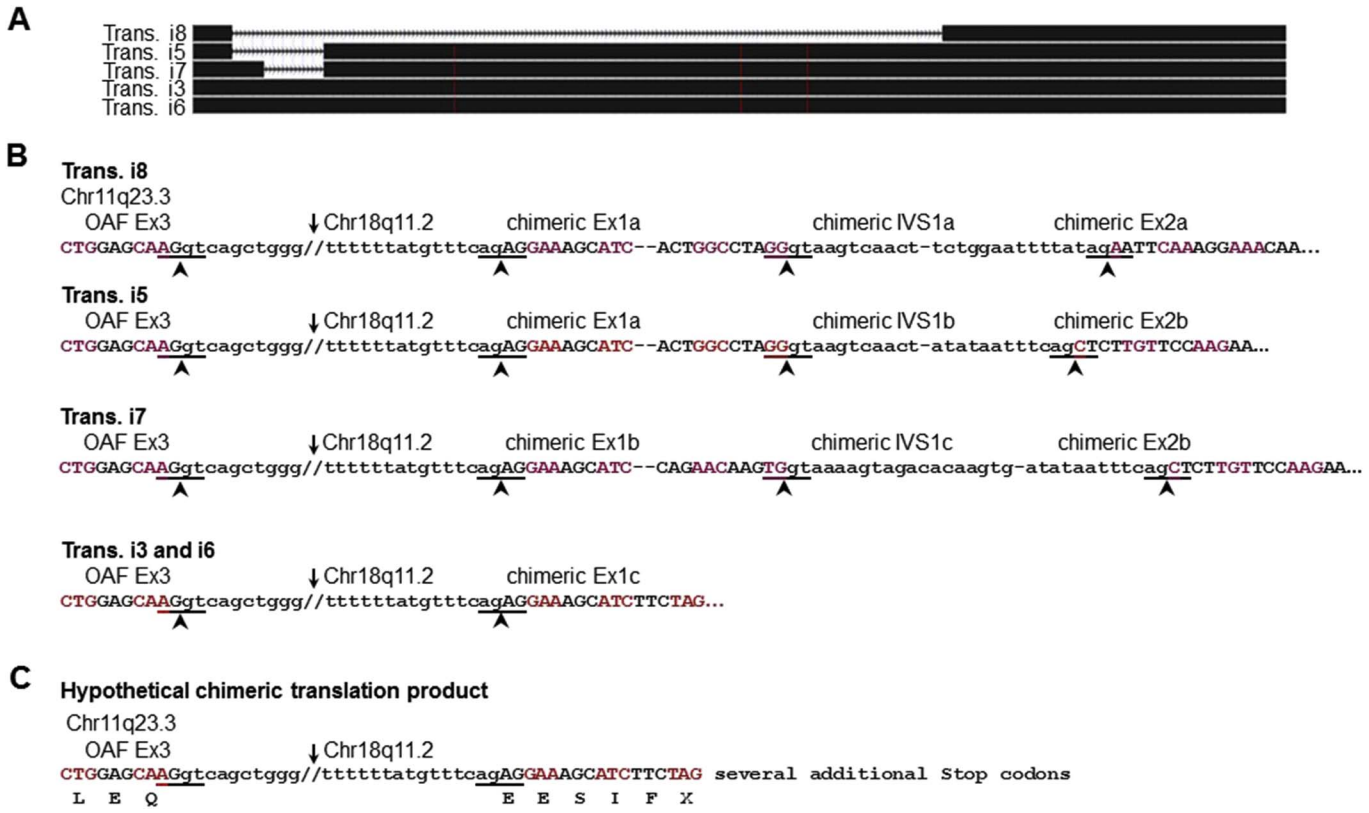

Fig. 5. Chimeric transcripts identified in LCLs by RNA CaptureSeq.
A)BLAT alignment of chimeric transcripts to the reference genome.
B) Schematic representation of the chimeric transcript isoforms. Coding and intronic sequences are in upper and lower case-letters, respectively. Coding triplets are highlighted in brown and black. Splice sites are indicated by arrowheads and underlined. The full-length fusion intronic sequence (//) is not shown and the breakpoint within this is depicted by the arrow. **C)** Hypothetical translation product of the chimeric transcripts.

cataract (Greenlees et al., 2015). Based on the available data we propose *PVRL1*, an interacting partner of *PVRL3*, as a major candidate gene, whose misregulation most likely contributes to the clinical phenotype described above. Therefore, we hypothesize that quantitative and spatiotemporal deregulation of *PVRL1* expression disturbs apex-apex junctions in target ocular and brain tissues affected by this anomaly (between anterior lens epithelium and fiber cells as well as of ciliary epithelia) leading to the KLD, EL and neurologic impairment. Adoption of *RBBP8* enhancers on the der(11) allele may represent the mechanism contributing to the misregulation of *PVRL1* expression (Supplementary Fig. S12).

The proposita does not present symptoms of conditions linked to dominantly inherited genes localized within the analyzed TADs from the breakpoint regions. Even *GATA6*, which is associated with congenital heart defects, has a haploinsufficiency index (HI) of 4.25, and is localized within the 18q11.2 brTAD, is most likely not involved in the phenotype (Supplementary Figs. S4 and S5). Corroborating this, non-pathogenic CNVs (both loss and gain) affecting *GATA6* as well as *MFRP, TECTA, PVRL1* have been reported (http://dgv.tcag.ca/gb2/gbrowse/dgv2_hg19/).

Clinical phenotypes associated with balanced translocations not leading to haploinsufficiency of a single gene are generally unique partially overlapping known syndromes. Regarding, the small-sized eyes with abnormally short axial length presented by the proposita, it partially overlaps the dysfunction of *MFRP*, which also causes deregulation of axial eye length. However, based on the lack of expression in the developing lens, *MFRP* is not proposed as a candidate gene. Furthermore, the ocular phenotype reported here is different from typical marfanoid eyes that usually are myopic, big and with increased axial length. Therefore, we conclude that the proposita has an asymmetric ASD in both eyes leading to KLD (OD) and EL (OS). We do not have any indication of a mechanical disturbance of the lens-corneal adhesion.

The extensive bioinformatics analyses of the reference TADs from each translocation breakpoint, despite highlighting gaps in our current knowledge regarding chromatin-interacting domains, support our conclusions. The analyzed TAD regions are considerably different not only between human cell lines but also between the two breakpoint regions. It seems reasonable to hypothesize that TADs with weak boundaries and excessive CTCF-binding sites throughout the domains, such as in the 11q23.3 region, are more prone to give rise to new TADs as a result of a chromosome rearrangement. Hypothetically, depending on the genomic content of the new TADs, these will be preferentially pathogenic.

As ocular tissue biopsies from the proposita were unavailable and data from LCLs may not reflect the spatial and temporal expression of the candidate genes during development, additional mouse models were used for developmental expression studies. As lens development progresses through embryonic, early post-natal and adult stages, *Oaf* expression is progressively elevated and is significantly enriched in the lens. On the other hand, *Pvrl1* is expressed, albeit at lower levels, at the ocular developmental stages relevant to the phenotype. Finally, the findings that lens epithelium, the tissue component that remains connected to the overlying cornea in type 2 PA, normally exhibits high *Oaf* expression and low *Pvrl1* expression in contrast to the proposita, who exhibits low *OAF* and high *PVRL1* expression, add further likelihood that disruption of *OAF* and deregulation of *PVRL1* contribute to the full manifestation of the phenotype. This may explain the failure of whole-exome sequence to identify isolated mutations within these genes in unrelated patients with PA (Weh et al., 2014).

The altered expression level of genes within the 11q23.3 breakpoint-spanning TAD suggests that we cannot exclude that other genes

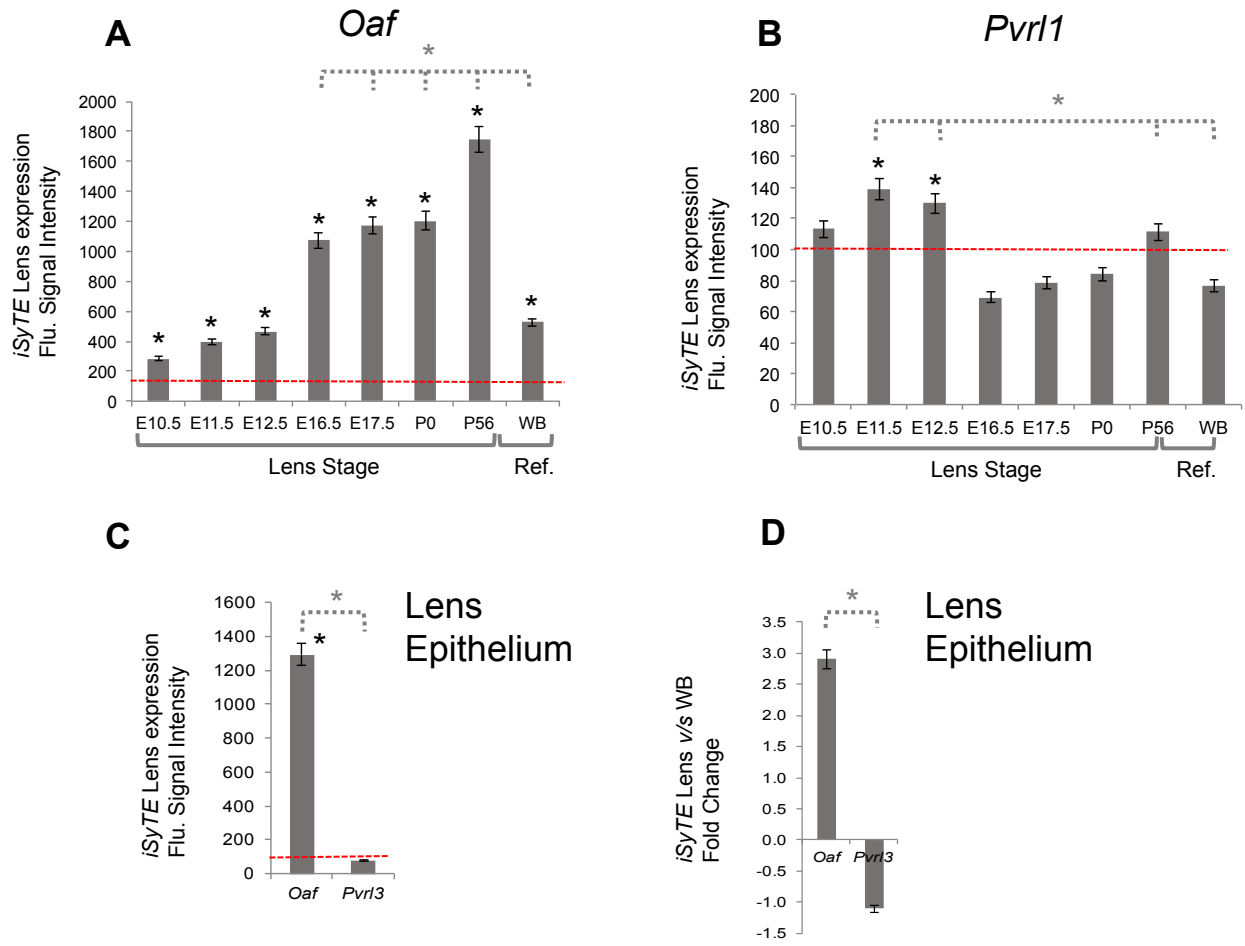

Fig. 6. Lens-specific expression patterns of the mouse orthologues of the *OAF* and *PVRL1* candidate genes. **A)** *Oaf* exhibits high expression (> 100 fluorescent probe binding intensity units, $p < .05$) in the developing lens starting from E10.5, when the lens vesicle is in the process of separating from the overlying ectoderm that will form the future cornea. Furthermore, its expression is progressively elevated through embryonic, early post-natal and adult stages (from E10.5 through P56). Compared to the whole embryonic tissue minus eyes (WB) reference dataset, *Oaf* expression is also progressively significantly enriched in the lens. **B)** *Pvrl1* is significantly expressed in mouse lens at E11.5-E12.5 and is down-regulated in later stages. It is enriched in the E11.5 and E12.5 lens compared to the WB reference dataset. **C)** *Oaf* exhibits high absolute microarray fluorescent expression intensities in isolated mouse lens epithelium at P28. **D)** *Oaf* is enriched at several-fold higher levels compared to *Pvrl1* in mouse lens epithelium. Error bars represent standard error of the mean (SEM). Red dotted line represents expression cut-offs at fluorescent probe intensity of 100. This cut-off is based on prior experience of independently validating candidate genes by alternate experiments. Asterisk (grey) represents significant differences between designated comparisons in lens stages with WB ($p < .05$). Asterisk (black) represents significant expression in the lens ($p < .05$).

from this region may also contribute to the clinical phenotype, including the neurological impairment observed in this subject.

It can be hypothesized that OAF, a protein present in the vitreous fluid, with high developmental expression during lens morphogenesis, and recently associated with corneal topography and disease, is required for normal separation of the cornea and lens tissues; moreover, elevated expression of *PVRL1*, coding for a cell-adhesion factor mediating apex-apex adhesion junctions in ocular and brain tissues, may lead to the persistence of the lenti-corneal stalk. Taken together, these findings suggest a cooperative role for OAF and PVRL1 in ocular development.

Research addressing clinically relevant ocular abnormalities associated with chromosome rearrangements provides valuable insights into gene action controlling eye development and, in this case, the development of the anterior chamber of the eye.

Disclosures and contributions

The authors declare that they have approved this article, and that they have no conflict of interest.

DD designed, oriented and analyzed the results, and wrote the manuscript; DA analyzed mouse lens expression array datasets; CA carried out RT-qPCR and sequencing of the junction fragments; BG and MD carried out RNA CaptureSeq analysis; JF performed Hi-C data analysis; LH, MP and LH submitted the samples and clinical ophthalmological examination of the proposita and her family members; JL contributed to the writing of the manuscript.

Acknowledgments

We are grateful to the family members for their involvement in this study. We thank the Chrombios Molecular Cytogenetics GmbH and the Gulbenkian Institute of Science for technical assistance. We thank Dominik Kaczorowski for preparation of RNA CaptureSeq libraries, Bárbara Marques for the fluorescence in situ hybridization (FISH) and Salil A. Lachke and Cynthia C. Morton for their valuable comments on the manuscript. CA was supported by a Ricardo Jorge Research Fellowship from Instituto Nacional de Saúde Dr Ricardo Jorge I.P. (Ref. BRJ/01/DG/2009). This research is supported by Fundação para a Ciência e a Tecnologia Research Grants PTDC/SAU-GMG/118140/2010 and HMSP-ICT/0016/2013.

Appendix A. Supplementary data

Supplementary data related to this article can be found at http://dx.doi.org/10.1016/j.exer.2017.12.012.

References

Agrawal, S.A., Anand, D., Siddam, A.D., et al., 2015. Compound mouse mutants of bZIP transcription factors Mafg and Mafk reveal a regulatory network of non-crystallin genes associated with cataract. Hum. Genet. 134, 717–735.

Bergstrom, D.E., Merli, C.A., Cygan, J.A., Shelby, R., Blackman, R.K., 1995. Regulatory autonomy and molecular characterization of the Drosophila out at first gene. Genetics 139, 1331–1346.

Chandra, A., Charteris, D., 2014. Molecular pathogenesis and management strategies of *ectopia lentis*. Eye 28, 162–168.

David, D., Cardoso, J., Marques, B., et al., 2003. Molecular characterization of a familial translocation implicates disruption of HDAC9 and possible position effect on TGFB2 in the pathogenesis of Peters' anomaly. Genomics 81, 489–503.

David, D., Marques, B., Ferreira, C., et al., 2013. Co-segregation of trichorhinophalangeal syndrome with a t(8;13)(q23.3;q21.31) familial translocation that appears to increase TRPS1 gene expression. Hum. Genet. 132, 1287–1299.

Doucette, L., Green, J., Fernandez, B., Johnson, G.J., Parfrey, P., Young, T.L., 2011. A novel, non-stop mutation in FOXE3 causes an autosomal dominant form of variable anterior segment dysgenesis including Peters anomaly. Eur. J. Hum. Genet. 19, 293–299.

Greenlees, R., Mihelec, M., Yousoof, S., et al., 2015. Mutations in SIPA1L3 cause eye defects through disruption of cell polarity and cytoskeleton organization. Hum. Mol. Genet. 24, 5789–5804.

Inagaki, M., Irie, K., Ishizaki, H., et al., 2005. Roles of cell-adhesion molecules nectin 1 and nectin 3 in ciliary body development. Development 132, 1525–1537.

Jamieson, R.V., Perveen, R., Kerr, B., et al., 2002. Domain disruption and mutation of the bZIP transcription factor, MAF, associated with cataract, ocular anterior segment dysgenesis and coloboma. Hum. Mol. Genet. 11, 33–42.

Kurilec, J.M., Zaidman, G.W., 2014. Incidence of Peters anomaly and congenital corneal opacities interfering with vision in the United States. Cornea 33, 848–850.

Lachke, S.A., Higgins, A.W., Inagaki, M., et al., 2012. The cell adhesion gene PVRL3 is associated with congenital ocular defects. Hum. Genet. 131, 235–250.

Li, J., Qin, Y., Zhao, F.K., et al., 2016. Anterior segment dysgenesis correlation with epithelial-mesenchymal transition in Smad4 knockout mice. Int. J. Ophthalmol. 9, 943–947.

Lupiáñez, D.G., Kraft, K., Heinrich, V., et al., 2015. Disruptions of topological chromatin domains cause pathogenic rewiring of gene-enhancer interactions. Cell 161, 1012–1025.

Mataftsi, A., Islam, L., Kelberman, D., Sowden, J.C., Nischal, K.K., 2011. Chromosome abnormalities and the genetics of congenital corneal opacification. Mol. Vis. 17, 1624–1640.

Mercer, T.R., Clark, M.B., Crawford, J., et al., 2014. Targeted sequencing for gene discovery and quantification using RNA CaptureSeq. Nat. Protoc. 9, 989–1009.

Mukai, M., Kitadate, Y., Arita, K., Shigenobu, S., Kobayashi, S., 2006. Expression of meiotic genes in the germline progenitors of Drosophila embryos. Gene Expr. Patterns 6, 256–266.

Mwenda, A.S., 2012. Peters anomaly with post axial polydactyly, bilateral camptodactyly and club foot in a Kenyan neonate: a case report. J. Med. Case Rep. 6, 16. http://dx.doi.org/10.1186/1752-1947-6-16.

Nischal, K.K., 2015. Genetics of congenital corneal opacification-impact on diagnosis and treatment. Cornea 34, S24–S34.

Ordulu, Z., Wong, K.E., Currall, B.B., et al., 2014. Describing sequencing results of structural chromosome rearrangements with a suggested next-generation cytogenetic nomenclature. Am. J. Hum. Genet. 94, 695–709.

Ozeki, H., Shirai, S., Nozaki, M., et al., 2000. Ocular and systemic features of Peters' anomaly. Graefes Arch. Clin. Exp. Ophthalmol. 238, 833–839.

Qvist, P., Huertas, P., Jimeno, S., et al., 2011. CtIP mutations cause Seckel and Jawad syndromes. PLoS Genet. 7 (10), e1002310.

Rao, S.S., Huntley, M.H., Durand, N.C., et al., 2014. A 3D map of the human genome at kilobase resolution reveals principles of chromatin looping. Cell 159, 1665–1680.

Redin, C., Brand, H., Collins, R.L., et al., 2017. The genomic landscape of balanced cytogenetic abnormalities associated with human congenital anomalies. Nat. Genet. 49, 36–45.

Summers, K.M., Withers, S.J., Gole, G.A., Piras, S., Taylor, P.J., 2008. Anterior segment mesenchymal dysgenesis in a large Australian family is associated with the recurrent 17 bp duplication in PITX3. Mol. Vis. 14, 2010–2015.

Suzuki, K., Hu, D., Bustos, T., et al., 2000. Mutations of PVRL1, encoding a cell-cell adhesion molecule/herpesvirus receptor, in cleft lip/palate-ectodermal dysplasia. Nature Genet. 25, 427–430.

Takai, Y., Shimizu, K., Ohtsuka, T., 2003. The roles of cadherins and nectins in interneuronal synapse formation. Curr. Opin. Neurobiol. 13, 520–526.

Vincent, A., Billingsley, G., Priston, M., et al., 2006. Further support of the role of CYP1B1 in patients with Peters anomaly. Mol. Vis. 12, 506–510.

Weh, E., Reis, L.M., Happ, H.C., et al., 2014. Whole-exome sequence analysis of Peters anomaly. Hum. Genet. 133, 1497–1511.

Zepeda-Mendoza, C.J., Ibn-Salem, J., Kammin, T., et al., 2017. Computational prediction of position effects of apparently balanced human chromosomal rearrangements. Am. J. Hum. Genet. 101, 206–217.